

## **Elastic wave-equation migration for laterally varying isotropic and HTI media**

Richard A. Bale and Gary F. Margrave

### **SUMMARY**

Prestack wave-equation migration of isotropic or anisotropic elastic seismic data is described as vector wavefield extrapolation, plus an imaging condition for combinations of shot and receiver wave-modes. For azimuthally anisotropic data, the effect is to combine the (normally separate) steps of shear-wave splitting correction and migration into a single migration step. This enables a more accurate correction of the shear waves based upon the local propagation direction. The algorithm is extended to laterally varying medium with two different forms of generalized phase shift operators. The first, which we call “phase shift plus adaptive windowing” (PSPAW), is appropriate for anisotropic media described by several parameters. The second, based on conventional phase shift plus interpolation (PSPI), has been formulated for isotropic media, but is computationally intractable for general anisotropic media. In both cases, the spatial interpolation methodology is applied both to the phase shift and to the modal decomposition and recomposition steps.

The PSPAW algorithm has been applied to modelled data, first for a faulted isotropic model, and then for a model with a faulted layer which is transversely isotropic with a horizontal symmetry axis (HTI). The anisotropic elastic migration unravels the effect of shear-wave splitting as a natural consequence, a task which we show isotropic migration fails to do.

The isotropic PSPI algorithm has recently been applied to a new elastic version of the well-known Marmousi model, to test the ability of this algorithm with highly variable media. The preliminary results are encouraging, especially for the shallow imaging of the converted wave data.

### **INTRODUCTION**

Imaging elastic data in the presence of azimuthal anisotropy, for example in vertically fractured reservoirs, is complicated by shear-wave splitting. Conventionally, this is tackled by horizontal component rotations to isolate the fast (S1) and slow (S2) shear waves. The separate S1 and S2 data may then be separately migrated, or simply recombined into a single shear-wave dataset after a vertical shift to align them before migration. There are some approximations implicit in this approach, which is essentially based on vertical propagation theory. For example, the rotation step assumes that the polarizations are orthogonal and lie within the horizontal plane. In fact for shear waves arriving at oblique angles the polarizations cannot be correctly handled by horizontal rotation, since they are not orthogonal within that plane. Furthermore, the shear-wave velocities for azimuthally anisotropic media are dependent on propagation direction. The “fast” and “slow” shear-wave velocities may even cross over at larger phase angles. There is no single static shift that will correctly align the two shear waves for all angles.

To overcome these limitations, the shear-wave rotation and shift operators should both be dependent upon phase angle. The central idea of this paper is to incorporate the correction for shear-wave splitting within the migration extrapolation. This contrasts with the usual approach, which treats them as two separate problems.

Wavefield extrapolation is at the heart of the class of migration algorithms commonly referred to as wave-equation migration. A wavefield extrapolator, as used in such migration schemes, generates the wavefield at depth  $z + \Delta z$  from the wavefield at depth  $z$ , given the medium parameters over the depth interval, such that the medium may be approximated as invariant with respect to  $z$  over the interval. In the derivation of a wavefield extrapolator, an important concept is the *one-way wave equation*. Use of a one-way wave equation avoids some of the complexity associated with multiple scattering, is more robust to velocity errors, and is in general more computationally efficient than methods based on the full two-way wave equation. In cases where the medium parameters depend upon depth alone, the (scalar) one-way wave equation can be derived by a simple factorization of the two-way wave equation in the frequency-wavenumber domain. This gives rise to a phase-shift algorithm. In more realistic cases where the medium varies laterally, a standard approach is to assume a solution of the same form, but where the velocity is a function of lateral position. This gives rise to pseudodifferential operator type methods, such as the generalized phase shift plus interpolation (GPSPI) algorithm, and the nonstationary phase shift (NSPS) algorithm (Margrave and Ferguson, 1999). The GPSPI algorithm is an analytic formulation of Gazdag and Sguazzero's (1984) PSPI algorithm; in GPSPI an extrapolation operator is designed uniquely for each output point.

The above remarks apply to scalar-wave equation extrapolators. Strictly speaking, these are only appropriate for migration in acoustic media. Nevertheless, they have been highly successful when applied to the migration of P-wave data obtained from conventional seismic surveys. Nevertheless, there are disadvantages in using a scalar-wave equation for extrapolating elastic-wave data. Firstly, the scalar-wave approach assumes that each wave-mode can be handled independently of the others, yet conversion between modes is commonplace. Secondly, scalar wavefield extrapolation cannot keep track of changes in polarization, which occur during wave propagation. Finally, it is difficult to account fully for effects of anisotropy, such as shear-wave splitting, using a scalar extrapolator. For these reasons it is preferable to approach elastic wavefield extrapolation from a *vector* (or, more accurately, *tensor*) wave equation standpoint.

In last years CREWES report we described an algorithm for extrapolation of elastic wavefields, and an extension to laterally variable media (Bale and Margrave, 2003a, 2003b). The laterally variable algorithm was formulated in terms of generalized PSPI (GPSPI) and NSPS type methods. The GPSPI version was actually implemented using fixed spatial windows.

After briefly reviewing the previous work, this paper will introduce two new algorithms for the extrapolation, and apply them within a prestack migration. First, we modify the GPSPI theory to get an adaptive extrapolation algorithm appropriate for anisotropic elastic media. We will refer to this as "phase shift plus adaptive windowing" (PSPAW). Second, we propose an alternative elastic PSPI extrapolator that is more

closely related to the standard PSPI algorithm of Gazdag and Sguazzero. This can be applied when the medium is *elastic* and *isotropic*. We then describe imaging conditions that can be used with either of these extrapolators in a prestack shot record migration. In other words, we are describing two related migration algorithms, where one is applicable to either isotropic or HTI media, and the other is optimized for isotropic media.

In the examples section, we test the anisotropic version of the migration on a synthetic model containing a faulted HTI layer. This more efficient isotropic migration code is also applied on a new elastic version of the well-known Marmousi model.

## THEORY

The theory required for elastic wavefield extrapolation is based on eigen-solutions to the Kelvin-Christoffel equation and the theory of anisotropic propagator matrices (Fryer and Frazer, 1984; 1987). For wave propagation in a 2-D, laterally homogeneous, HTI medium with horizontal slowness  $p_x = k_x/\omega$ , the elastic extrapolation operator is

$$\mathbf{b}(p_x, z_{n+1}, \omega) = \mathbf{D}_n e^{i\omega \Lambda_n (z_{n+1} - z_n)} \mathbf{D}_n^{-1} \mathbf{b}(p_x, z_n, \omega), \quad (1)$$

where  $\mathbf{b}$  is a vector containing displacement  $\mathbf{u}$ , and the (scaled) vertical traction  $\boldsymbol{\tau}$ . It is given by

$$\mathbf{b} = \begin{pmatrix} \mathbf{u} \\ \boldsymbol{\tau} \end{pmatrix},$$

where

$$\boldsymbol{\tau} = -\frac{1}{i\omega} (\sigma_{13} \quad \sigma_{23} \quad \sigma_{33})^T.$$

The diagonal matrix  $\Lambda_n = \text{diag}(q_n^P \quad q_n^{S1} \quad q_n^{S2})$  contains the vertical slownesses for each mode in layer  $n$ . In the HTI case, the squared slownesses can be analytically determined from the solution of one quadratic and one linear equation (the choice of sign for the square root is based upon whether an up- or down- going solution is required). The 6-by-3 matrix  $\mathbf{D}_n$  contains the eigenvectors,  $\hat{\mathbf{b}}_n^{(M)}$ , for each mode, (quasi-) P, S1 and S2, which are solutions to the one-way wave equation  $\partial \mathbf{b} / \partial z = i\omega \mathbf{A} \mathbf{b}$  in layer  $n$ .  $\mathbf{A}$  is referred to as the system matrix in geophysical propagator matrix theory (e.g. Fryer and Frazer, 1984). In the mechanics literature it is referred to as the fundamental elasticity matrix (e.g. Ting, 1996, p145). The components of  $\mathbf{A}$  are functions of the elastic constants, horizontal slowness, and frequency. It embodies a combination of the stress-strain relationship (generalized Hooke's Law) and Newton's equation of motion. Layer  $n$  lies between  $z_n$  and  $z_{n+1}$ . Both  $\mathbf{D}_n$  and  $\Lambda_n$  depend on  $p_x$ , but not on  $\omega$ , nor on  $x$ , in this case.

In words, equation (1) states the following: decompose the displacement-stress wavefield at depth  $z_n$  into the three eigenstates for layer  $n$  which are the elastic modes; propagate each mode using the vertical slowness for that mode; recombine the modes at the new depth  $z_{n+1}$ . The vector  $\mathbf{b}$  is, by design, continuous in the presence of medium

discontinuities between horizontal layers. Therefore, we may proceed using the extrapolated  $\mathbf{b}$  as the boundary condition for the next depth step.

We now consider generalization of the above to spatially variable media. The key modifications are that  $\Lambda_n$  and  $\mathbf{D}_n$  now depend on both  $p_x$  and  $x$ . The GPSPI form of equation (1) is

$$\mathbf{b}_{GPSPI}(x, z_{n+1}, \omega) = \frac{\omega}{2\pi} \int_{-\infty}^{\infty} \mathbf{D}_n(x, p_x) \mathbf{E}_n(x, p_x, \omega) \times \mathbf{D}_n^{-1}(x, p_x) \mathbf{b}(p_x, z_n, \omega) e^{-i\omega p_x x} dp_x, \quad (2)$$

where

$$\mathbf{b}(p_x, z_n, \omega) = \int_{-\infty}^{\infty} \mathbf{b}(x, z_n, \omega) e^{i\omega p_x x} dx,$$

and

$$\mathbf{E}_n(x, p_x, \omega) = e^{i\omega \Lambda_n(x, p_x)(z_{n+1} - z_n)}.$$

Equation (2) can be considered as a Fourier integral operator in the standard (Kohn Nirenberg) calculus. An anti-standard (adjoint) form of equation (2) can also be written, describing NSPS elastic wavefield extrapolation (Bale and Margrave, 2003b). Of course, this generalization is approximate and accounts only for one-way wavefield transmission effects. Mode conversion can only occur at the horizontal boundaries represented by the depth steps in our marching algorithm. A dipping boundary is in effect approximated by a "staircase" of horizontal boundaries. Whether or not we have made a useful approximation to the complete elastic migration problem will be only become clear after much algorithmic testing.

### Adaptive windowing algorithm: PSPAW

Equation (2) as written is very expensive, since it is not an inverse Fourier transform, but rather a Fourier integral operator and therefore cannot be performed using an FFT. A practical implementation of this equation involves some form of windowing or interpolation. The traditional PSPI approach (Gazdag and Sguazzero, 1984) is to compute several wavefields with reference velocities, return each to the spatial domain with inverse FFTs, and interpolate the results. An alternative approach, which we refer to as "phase shift plus windowing" (PSPW), uses spatial windowing operators applied to the inverse transformed data. In the case of anisotropic elastic wavefield extrapolation, the traditional approach has a major drawback, which we now explain.

The minimum number of parameters required to represent an HTI medium is six, which can be defined (among various equivalent ways) as:  $\alpha_0, \beta_0$ , the P- and S-wave velocities for propagation along the symmetry axis;  $\epsilon, \delta, \gamma$ , the Thomsen parameters; and  $\phi$ , the orientation of the axis of symmetry within the horizontal plane. If we assume that only 5 reference values are selected for each parameter, then the total number of reference operators required is  $5^6 = 15625$ . This is clearly intractable, unless the

dependence on the parameters is somehow decoupled. In general this is not possible. In the next section we examine the special case of an isotropic medium, where the parameter dependence is approximately separable. Here, we focus on the spatial windowing approach instead.

We use a variation of PSPW with variable size windows, which we call “phase shift plus adaptive windowing” (PSPAW). The PSPAW algorithm is related to the adaptive Gabor method (Grossman et al., 2002), although the Gabor transform is not actually used here. In PSPAW, spatial windows are constructed by combining elementary small windows, called “atoms”, into larger windows, referred to as “molecules”. The molecules are built up along the horizontal spatial direction until some acceptance criterion is violated. At this point a new molecule is started. In this way, large windows are used when the velocity variation is mild, but smaller windows are used in areas of rapid variation. For the scalar extrapolation of Grossman et al., the acceptance criterion is based on changes in velocity. For the elastic HTI case we are considering here, this is not possible, because there are 3 modes, each with a velocity which depends upon phase angle. Instead we apply the following procedure:

1. Phase slowness is computed for P, S1 and S2 modes, for a fixed set of phase angles using the anisotropic parameters at the spatial center of each atom.
2. Within each molecule, a record is kept of the average, minimum and maximum phase slownesses, for each phase angle. The average is computed using Schoenberg and Muir’s (1989) calculus for addition of anisotropic layers. In addition, the average, minimum and maximum symmetry-axis azimuths are recorded.
3. A new atom is accepted to the current molecule on condition that including it does not cause the range between minimum and maximum slowness to exceed some limit, for any mode. This limit is determined by requiring that the maximum phase error does not exceed one-half a cycle, at the maximum frequency, over the entire depth range.
4. A new atom is accepted only if the symmetry axis variation within the molecule will remain less than some specified limit (we use  $10^\circ$ ).
5. If either criteria in 3 or 4 are violated a new molecule is created starting with the current atom.

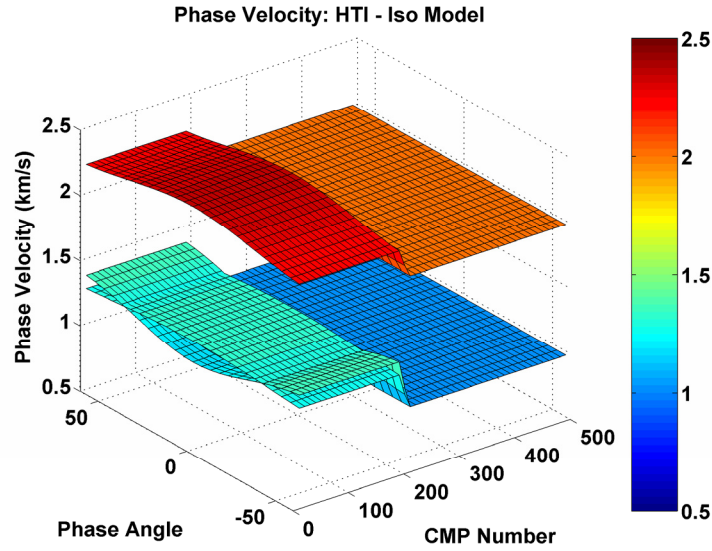


FIG. 1. Phase velocity curves as a function of horizontal position and phase angle for a depth step which transitions from an HTI medium (left) to an isotropic medium (right). Upper sheet is the P-wave slowness, lower sheets are S1 and S2 slownesses.

Step 1 is illustrated in Figure 1, displayed as phase velocity instead of slowness. For the isotropic part of the model, to the right, the P velocity is constant with phase angle, and both S velocities are equal and constant. For the HTI part, to the left, there are variations in all three velocities with phase angle, and the separation of S1 and S2 velocities is evident.

Step 4 is important for two reasons. First, it does not make sense to compare two S1 or two S2 phase slowness curves from nearby positions, unless the two symmetry axes are also closely aligned. Second, the decomposition and recombination matrices  $\mathbf{D}_n^{-1}$  and  $\mathbf{D}_n$  in equation (2) are also subject to spatial variation, which depends on both the velocities and also the orientation of the symmetry axis.

### Alternative algorithm for isotropic media: PSPI

In the special case of an isotropic medium with constant  $V_p/V_s$  ratio, the polarizations and phase shifts employed in equation (2) can be controlled for each mode by a single parameter. In particular, the vertical slownesses (which determine the phase shifts) for P-wave and S-wave modes are

$$q^P = \sqrt{1/\alpha^2 - p_x^2} \tag{3a}$$

and 
$$q^{S1} = q^{S2} = \sqrt{1/\beta^2 - p_x^2} \tag{3b}$$

where  $\alpha$  and  $\beta$  are the P-wave and S-wave velocities for the layer in question (we drop the layer suffix, which is superfluous here).

The P-wave and SV-wave eigenvectors for an isotropic recomposition matrix  $\mathbf{D}_n$  are calculated in Appendix A. The P-wave eigenvector depends on the S-wave velocity as well as the P-wave velocity. In contrast, the S-wave eigenvector depends only on the S-wave velocity.

If we assume the  $V_p/V_s$  ratio is constant within each layer then each eigenvector is controlled by a single parameter – the velocity of the corresponding wave-mode. In this case, we can employ a “conventional” PSPI approach as follows:

1. Choose  $N$  reference P-wave velocities  $\{\alpha_1, \alpha_2, \alpha_3, \dots, \alpha_N\}$  and define  $N$  reference S-wave velocities based on the constant  $V_p/V_s$  ratio,  $\gamma_0$ , by  $\beta_J = \alpha_J/\gamma_0$  for  $J = 1, \dots, N$ .
2. For each reference P-wave velocity, decompose the wavefield using the decomposition matrix designed with that velocity.
3. Extrapolate P-wave and S-wave wavefields using the appropriate vertical slowness for that mode.
4. Interpolate the results for both P and S wavefields at each output location based upon local velocity, and the two bracketing reference velocities for each mode.

Even if the  $V_p/V_s$  ratio varies within the layer, the above algorithm, with some modifications, will still be accurate for all steps except for computing the P-wave amplitudes. We begin by computing the  $V_p/V_s$  ratio based upon the ratio of mean P- and S-wave velocities,  $\bar{\alpha}$  and  $\bar{\beta}$ , over the aperture of the migration for each shot.

$$\gamma_{ave} = \bar{\alpha}/\bar{\beta} \quad (4)$$

Next, we adjust the range of P- and S-wave velocities as follows:

$$\begin{aligned} \alpha_{min} &\leftarrow \min(\alpha_{min}, \gamma_{ave}\beta_{min}) \\ \beta_{min} &\leftarrow \min(\alpha_{min}/\gamma_{ave}, \beta_{min}) \\ \alpha_{max} &\leftarrow \max(\alpha_{max}, \gamma_{ave}\beta_{max}) \\ \beta_{max} &\leftarrow \max(\alpha_{max}/\gamma_{ave}, \beta_{max}) \end{aligned} \quad (5)$$

This is done to ensure that the reference velocities chosen are matched via a constant  $V_p/V_s$  ratio.

The P and S reference velocities are then selected based upon the harmonic sampling criteria of Gazdag and Sguazzero (1984). Since the actual  $V_p/V_s$  ratio varies laterally, the interpolation of P- and S-wave wavefields does not always use the corresponding reference values. For example, the P-wave might be interpolated using reference (P-wave) velocities  $J$  and  $J+1$ , whereas the S-wave might be interpolated using reference (S-

wave) velocities  $K$  and  $K+1$ . This is possible since the phase shifts dependence on velocity is decoupled.

For the modal decomposition and recomposition, with variable  $V_p/V_s$ , the situation is more complicated. The composition matrix depends on both P and S velocities. We do not want to compute  $N^2$  versions of  $\mathbf{D}_n$  and  $\mathbf{D}_n^{-1}$  corresponding to every possible combination of P and S velocity, which would be prohibitively expensive. Instead we use corresponding reference velocities, so that the  $V_p/V_s$  ratio is always  $\gamma_{ave}$ . In addition, we keep track of distinct displacement-traction vectors  $\mathbf{b}_p$  and  $\mathbf{b}_{SH}$ ,  $\mathbf{b}_{SV}$ , enabling the appropriate local velocity to be employed for each mode as described in Appendix B.

In the case of the P-wave, this will result in a slight error, since the decomposition matrix includes a dependence on the  $V_p/V_s$  ratio. Numerical tests indicate that this error is relatively small for reasonable variation of  $V_p/V_s$ .

### Imaging Conditions

During elastic wavefield extrapolation the displacement wavefield is decomposed into three wave-modes P, S1 and S2, in each layer. For the forward extrapolation of the down-going wavefield from the source, these are given by the vector of wave-mode amplitudes

$$\mathbf{w}_D = \begin{pmatrix} w_P^D & w_{S1}^D & w_{S2}^D \end{pmatrix}^T = \mathbf{D}_D^{-1} \mathbf{b}_{D,src}. \quad (6)$$

For backward extrapolation of the up-going wavefield from the receiver, they are given by the wave-mode vector

$$\mathbf{v}_U = \begin{pmatrix} v_P^U & v_{S1}^U & v_{S2}^U \end{pmatrix}^T = \mathbf{D}_U^{-1} \mathbf{b}_{U,rcv}. \quad (7)$$

In these and subsequent equations, the layer subscript  $n$  is omitted, while sub- and superscripts  $U$ ,  $D$ ,  $src$  and  $rcv$  are used to distinguish up- from down-going, and shot from receiver wavefields. The wave-mode amplitude wavefields,  $\mathbf{w}_D$  and  $\mathbf{v}_U$  are byproducts of the extrapolation of shot and receiver wavefields using equations (1) or (2).

The goal of elastic migration, assuming a P-wave source, is to produce images corresponding to P-P reflectivity, and P-S reflectivity for the isotropic case, or P-S1 and P-S2 reflectivity for the HTI case. (Additional images such as S1-S2 are also possible, if the source generates shear energy.) To obtain these images we must apply an imaging condition. A *correlation* imaging condition between the corresponding elements of equations (3) and (4) is written

$$I_{MN}^{corr.}(x, z) = \int_0^{\omega_{max}} \overline{w}_M^D(x, z, \omega) v_N^U(x, z, \omega) d\omega, \quad (8)$$

where  $I_{MN}$  is the image for down-going mode  $M$ , and up-going mode  $N$ , where  $M, N \in \{P, S1, S2\}$ . The overscore here denotes complex conjugation.

A *deconvolution* imaging condition is written

$$I_{MN}^{decon.}(x, z) = \int_0^{\omega_{max}} \frac{\overline{w}_M^D(x, z, \omega) v_N^U(x, z, \omega)}{|w_M^D(x, z, \omega)|^2 + \varepsilon} d\omega, \quad (9)$$

where the division is stabilized by the addition of the small real value,  $\varepsilon$ .

The deconvolution imaging condition is used in our examples.

### Other considerations

Both the PSPI and PSPAW algorithms described above are implemented with a split-step correction (Stoffa et al., 1990). The split-step correction improves the accuracy of extrapolation for small angles. This is done by applying a residual phase shift in the spatial domain to correct for the difference between the reference and actual velocities. This is also referred to as the “thin-lens” correction. We also apply a related wavefield interpolation as described by Fu (2004) to enable image output at finer depth sampling than the extrapolation step.

As pointed out in Zhang et al. (2003) there is an often neglected operator aliasing effect in prestack wave-equation migration. We correct for this effect by generating output at half of the receiver interval, so that the spatial Nyquist wavenumber for the image is twice that of the extrapolated wavefields.

## EXAMPLES

### Isotropic and HTI model with fault

The elastic wave-equation migration using the adaptive PSPI algorithm was tested on the isotropic model shown in Figure 2. It was then tested on a second model which is identical, except that the second, faulted layer is an HTI medium with a symmetry axis at  $45^\circ$  to the inline direction.. The input data for these tests were generated with a 2-D anisotropic pseudospectral modelling code (Bale, 2003), using a P-wave source and 3-component receivers. The source signature used was a zero phase Ricker wavelet with 15Hz center frequency.

The results of elastic migration on the isotropic dataset are shown in Figure 3. The shot spacing was 200m, from 160m to 4960m. The receiver range is from 565m to 4555m along the surface. Apart from better resolution on the PS section as anticipated,

the images are generally in good agreement. The phase rotation present on the PS reflection is, we believe, a result of a polarity change at large offset.

Figure 4 shows the result of elastic migration applied to the HTI dataset. The data were modeled using identical geometry to that used for the isotropic case. For this particular case, we generate two separate PS images, one for the fast (S1) mode and one for the slow (S2) mode. For isotropic layers, the SV mode is assigned to the S2 section. An interesting aspect is that the S1 mode only responds to the top and bottom of the HTI layer. It does not respond to any other interfaces – hence the absence of the flat basement reflector on the second image.

Figure 5 shows the result of applying isotropic migration to the same data as used in Figure 4. The velocity model was constructed by replacing the HTI layer of the true model with an isotropic layer having the fastest velocity for each mode. The amplitudes are scaled as in Figure 4. In addition to some loss of amplitude, which we ascribe to uncorrected interference between the S1 and S2 modes, there is a residual basement reflection on the S1 section (which corresponds to SH-wave polarization for the isotropic model). This results from incorrect treatment of the polarization within the overlying HTI medium.

### **Elastic Marmousi model**

The last example is the elastic Marmousi-2 model, which is isotropic but highly heterogeneous. The Marmousi-2 dataset was generated by the Allied Geophysical Laboratory at the University of Houston (Martin et al., 2002). It is based upon the standard acoustic Marmousi model but with several modifications and extensions. Firstly, it has been extended laterally to a total line length of 17 km. The extensions are less structurally complex than the central section, but include interesting stratigraphic features and hydrocarbon accumulations. Secondly, it has been submerged under 500 m of water. Finally, it is an elastic model with density and shear velocity determined from empirical rock physics equations (Castagna et al., 1993; Greenburg and Castagna, 1992). The modelled data are very rich including both OBC and towed streamer data. We have confined our attention to the X and Z components of the OBC dataset.

We made use of the specialized isotropic version of the PSPI migration, as described above, to image this data. Testing on this dataset is ongoing. The results included within this report are of a preliminary nature. In particular, the central area poses imaging problems which have yet to be resolved. There are also very problematic water layer multiples in the data. Nevertheless we feel these results are interesting enough to include here. We focus on two parts of the model. The first corresponds to approximately the original Marmousi model, with much structural complexity, and velocity heterogeneity. The second part is a more stratigraphic area in the shallow part of the model.

Figure 6 shows the P-wave (a) and S-wave (b) impedance sections in the central section, roughly equivalent to the original Marmousi area. The water layer is not shown.

Figure 7 shows the P-P and P-S migrated images for this section of the model. Both images suffer somewhat from the presence of water layer multiples, and some aliased

diffraction noise from the water bottom. In this regard the P-P image is more affected by the multiples. Generally speaking, the P-P image is promising, whereas the P-S image is less clearly defined

Figure 8 shows the P- and S-wave impedance sections from a shallow, stratigraphic portion of the model. This is located to the left of the area shown in Figure 6. This area is considerably less structured, and the horizontal scale in figure 8 has been compressed for display.

Figure 9 shows the corresponding P-P and P-S migrated images. As seen in figure 9(b), the shallow P-S imaging is remarkable, displaying clear resolution advantages over the equivalent P-P section in figure 9(b). This is anticipated from theory, due to the slower S-wave velocities, but is striking nonetheless. Also of interest are the very different responses to the gas sand at 0.6km depth to the left of the image. The over-migration of the P-P gas sand is not fully understood at present. However, the reader should be aware that the effect is exaggerated by the very high amplitudes of the P-P response to the sand, compared to the relatively low amplitude response on the P-S image. Significantly, the ability of elastic wave data to provide discrimination between lithology and fluid is exhibited clearly in this example.

## CONCLUSIONS

We have developed wave-equation migration for elastic seismic data using two related elastic wavefield extrapolators.

The first, which we call PSPAW, is applicable in the presence of anisotropy. We have specifically implemented it for HTI media, such as may be encountered in vertically fractured reservoirs. The algorithm naturally focuses the separate S1 and S2 wavefields associated with shear-wave splitting, a task which isotropic migration cannot achieve. By using an extension of the generalized PSPI method, we are able to accommodate lateral variations in the velocities, as well as the degree and orientation of the anisotropy. This is done in an efficient way using an adaptive design. This employs as few operators as possible whilst satisfying a phase error criterion. We have demonstrated the migration on two examples: one isotropic, and one containing an HTI layer. The second example illustrates the ability of the migration to isolate the reflections arising from the top and bottom of the HTI layer on the S1 and S2 components. We show that using isotropic migration applied to data generated with an HTI model produces residual reflections with incorrect polarization.

The second extrapolator is essentially a conventional PSPI algorithm applied to both phase shift operators and modal composition/decomposition operators. The key is to decouple the dependence on the medium parameters. This appears only to be possible for isotropic media, and in this case an approximation is required for the P-wave modes. It is exactly correct for constant  $V_p/V_s$ . This algorithm appears to do a reasonable job on the isotropic, but highly variable, Marmousi-II elastic dataset. There are a number of extraneous issues with these data, primarily related to the water layer, which still need

attention. There also appears to be room for improvement in imaging the converted waves in the most structural part of the data.

### ACKNOWLEDGEMENTS

The authors gratefully acknowledge the generous support of the sponsors of CREWES and the POTSI (Pseudodifferential Operator Theory and Seismic Imaging) Consortium. We also acknowledge the Allied Geophysical Laboratory, at the University of Houston for permission to use the Marmousi II data, and in particular Prof. Robert Wiley and Gary Martin of GX technology for their support and advice regarding the dataset.

We thank Hugh Geiger and Jeff Grossman for valuable discussions. We especially thank Kevin Hall for his tireless help with the Marmousi-II data and hardware issues.

### REFERENCES

- Bale, R.A., 2003, Modeling 3D anisotropic elastic data using the pseudospectral approach: 65th Mtg., Eur. Assn. Expl. Geophys., Extended Abstracts.
- Bale, R.A., and Margrave, G.F., 2003a, Elastic wavefield extrapolation in HTI media: CREWES Research Report, **15**.
- Bale, R.A. and Margrave, G.F., 2003b, Adapting elastic wavefield extrapolation to laterally varying HTI media: CREWES Research Report, **15**.
- Castagna, J.P., Batzle, M.L., and Kan, T.K., 1993, Rock Physics – The link between rock properties and AVO response: in Castagna, J.P., and Backus, M.M., eds., Offset dependent reflectivity – Theory and practice of AVO anomalies, Society of Exploration Geophysics. Investigations in Geophysics no. 8, 135-171.
- Fryer, G.J., and Frazer, L.N., 1984, Seismic waves in stratified anisotropic media: Geophys. J. Roy. Astr. Soc., **78**, 691-710.
- Fryer, G.J., and Frazer, L.N., 1987, Seismic waves in stratified anisotropic media—II. Elastodynamic eigensolutions for some anisotropic systems: Geophys. J. Roy. Astr. Soc., **91**, 73-101.
- Fu, L-Y, 2004, Wavefield interpolation in the Fourier wavefield extrapolation: Geophysics, **69**, 257-264.
- Gazdag, J., and Sguazero, P., 1984, Migration of seismic data by phase shift plus interpolation: Geophysics, **49**, 124-131.
- Greenburg, M.L., and Castagna, J.P., 1992, Shear-wave velocity estimation in porous rocks: Theoretical formulation, preliminary verification and applications, Geophysical Prospecting, **40**, 195-210.
- Grossman, J.P., Margrave, G.F., and Lamoureux, M.P., 2002, Fast wavefield extrapolation by phase-shift in the nonuniform Gabor domain: CREWES Research Report, **14**.
- Margrave, G.F., and Ferguson, R.J., 1999, Wavefield extrapolation by nonstationary phase shift: Geophysics, **64**, 1067-1078.
- Martin, G., Larsen, S. and Marfurt, K., 2002, Marmousi-2: an updated model for the investigation of AVO in structurally complex areas, 72nd Ann. Internat. Mtg: Soc. of Expl. Geophys., 1979-1982.
- Schoenberg, M., and Muir, F., 1989, A calculus for finely layered anisotropic media: Geophysics, **54**: 581-589.
- Stoffa, P.L., Fakkema, J.T., de Luna Freire, R.M., and Kessinger, W. P., 1990, Split-step Fourier migration: Geophysics, **55**, 410-421.
- Ting, T.C.T., 1996, Anisotropic Elasticity: Theory and Applications, Oxford University Press.
- Zhang, Y., Sun, J., and Gray, S.H., 2003, Aliasing in wavefield extrapolation prestack migration: Geophysics, **68**, 629-633.

## APPENDIX A: ISOTROPIC MEDIA DECOMPOSITION MATRIX

In this appendix we evaluate the decomposition matrix for isotropic media and show that the decomposition for each mode depends only on two parameters, one of which is the  $V_p/V_s$  ratio. To simplify notation we drop the layer index, and write the recomposition and decomposition matrices as  $\mathbf{D}$  and  $\mathbf{D}^{-1}$ .

$\mathbf{D}$  is constructed from the eigenvectors

$$\hat{\mathbf{b}}_i = \varepsilon_i \begin{pmatrix} \mathbf{u}_i \\ \boldsymbol{\tau}_i \end{pmatrix}, \quad i = 1, \dots, 6. \quad (\text{A1})$$

where the  $\mathbf{u}_i$  are found by solving the Kelvin-Christoffel equation, and the  $\boldsymbol{\tau}_i$  are related to them through the stress-strain relationship. The  $\varepsilon_i$  are normalization constants. The 6 indices correspond to different modes with up and down-going wave directions. See Bale and Margrave (2003a), and references therein for details.

Once  $\mathbf{D}$  is known, the decomposition matrix is given simply by

$$\mathbf{D}^{-1} = (\mathbf{J}\mathbf{D})^T, \quad (\text{A2})$$

where

$$\mathbf{J} \equiv \begin{pmatrix} \mathbf{0}_3 & \mathbf{I}_3 \\ \mathbf{I}_3 & \mathbf{0}_3 \end{pmatrix}.$$

We consider only the down-going waves in the following analysis. Similar analysis applies to the up-going waves. In the isotropic case, using a coordinate frame such that SV modes are polarized in the x-z plane, the displacement eigenvector associated with the down-going P-wave is

$$\mathbf{u}_p^D = \alpha \begin{pmatrix} p_x \\ 0 \\ q_p \end{pmatrix}, \quad (\text{A3a})$$

where  $\alpha$  is the P-wave velocity,  $p_x$  is the horizontal slowness, and  $q_p$  is the vertical slowness for the P-wave.

The corresponding traction eigenvector is

$$\boldsymbol{\tau}_p^D = -\alpha\rho \begin{pmatrix} 2\beta^2 p_x q_p \\ 0 \\ 1 - 2\beta^2 p_x^2 \end{pmatrix}, \quad (\text{A3b})$$

where  $\rho$  is density and  $\beta$  is the S-wave velocity.

For the SV wave-mode the corresponding eigenvectors are:

$$\mathbf{u}_{SV}^D = \beta \begin{pmatrix} q_s \\ 0 \\ -p_x \end{pmatrix} \text{ and } \boldsymbol{\tau}_{SV}^D = -\beta \rho \begin{pmatrix} \beta^2(q_s^2 - p_x^2) \\ 0 \\ -2\beta^2 p_x q_s \end{pmatrix}, \quad (\text{A4})$$

where  $q_s$  is the vertical slowness for the S-waves (SV or SH).

For isotropic propagation the SH-wave is completely decoupled from the P- and SV-waves, and can be independently extrapolated.

Because of the simple form of the decomposition matrix in equation (A2), the above P and SV eigenvectors define fully the decomposition for the corresponding modes.

Equation (A3) shows that even though the displacement eigenvector for the P-wave is independent of the S-wave velocity, the traction vector is not. Therefore, the complete eigenvector  $\hat{\mathbf{b}}_P^D$ , a column vector of  $\mathbf{D}$ , is dependent on the S-wave velocity. So is the corresponding row-vector in the decomposition matrix  $\mathbf{D}^{-1}$ . This implies that we cannot exactly decouple the handling of P- and S-waves within the decomposition and recomposition steps. However, in the case that  $\alpha = \gamma_0 \beta$ , with  $\gamma_0$ , the  $V_P/V_S$  ratio, being constant for a given layer, we can replace the dependence on  $\beta$  in equation (A3b) with a further dependence on  $\alpha$ .

Surprisingly perhaps, the S-wave eigenvectors given in equation (A4) are *not* dependent on the P-wave velocity.

## APPENDIX B: MULTIPLE REFERENCE VELOCITY COMPOSITION- DECOMPOSITION

We write the composition equation in the following form:

$$\begin{aligned} \mathbf{b} &= \mathbf{D}\mathbf{v} \\ &= \left( \hat{\mathbf{b}}_P \quad \hat{\mathbf{b}}_{SH} \quad \hat{\mathbf{b}}_{SV} \right) \begin{pmatrix} v_P \\ v_{SH} \\ v_{SV} \end{pmatrix}, \\ &= \mathbf{b}_P + \mathbf{b}_{SH} + \mathbf{b}_{SV} \end{aligned} \quad (\text{B1})$$

where only the down-going (or up-going) waves are considered (omitting the U or D superscript for brevity), where the vector  $\mathbf{v}$  consists of the wave-mode amplitudes, and  $\mathbf{b}_M = v_M \hat{\mathbf{b}}_M$  for  $M \in \{P, SH, SV\}$ . The qualifiers SH and SV are used rather than S1 and S2, since isotropy is assumed here. For more details on the composition equation (B1) and the corresponding decomposition equation (B3) see Bale and Margrave (2003a) and references therein.

The wave-mode specific displacement-stress vectors  $\mathbf{b}_P, \mathbf{b}_{SH}$  and  $\mathbf{b}_{SV}$  are stored separately. Since the spatial variation of P- and S-wave velocities is not necessarily with a constant ratio, at any given output location  $x$  the total displacement-stress vector  $\mathbf{b}(x, z, \omega)$ , a combination of these vectors, will be obtained using different reference values.

For example, assume a set of reference media  $J = 1, \dots, N$  such that  $\alpha_J = \gamma_{ave} \beta_J$ . Define the reference vectors using (B1) with each reference medium as  $\mathbf{b}_{P,J}$  and  $\mathbf{b}_{SV,J}$  ( $\mathbf{b}_{SH}$  is independent of any parameters – and can be completely decoupled). Suppose at  $x = x_0$ , the local P-wave velocity  $\alpha$  is between  $\alpha_J$  and  $\alpha_{J+1}$ , whereas the S-wave velocity  $\beta$  is between  $\beta_K$  and  $\beta_{K+1}$ , with  $J \neq K$ . Then we have:

$$\mathbf{b}_P(x, z, \omega) = \lambda_P \mathbf{b}_{P,J} + (1 - \lambda_P) \mathbf{b}_{P,J+1}, \quad (\text{B2a})$$

and 
$$\mathbf{b}_{SV}(x, z, \omega) = \lambda_S \mathbf{b}_{SV,K} + (1 - \lambda_S) \mathbf{b}_{SV,K+1}, \quad (\text{B2b})$$

where 
$$\lambda_P = \frac{\alpha_{J+1} - \alpha}{\alpha_{J+1} - \alpha_J} \quad \text{and} \quad \lambda_S = \frac{\beta_{K+1} - \beta}{\beta_{K+1} - \beta_K}.$$

As noted in appendix A, the vectors  $\hat{\mathbf{b}}_P$  depend on both  $\alpha$  and  $\beta$ , whereas the vectors  $\hat{\mathbf{b}}_{SV}$  only depend upon  $\beta$ . So the only approximation involved in the above is using  $\beta_J$  rather than  $\beta_K$  within equation (B2a). If the variation of  $V_P / V_S$  is not large, the error involved can be expected to be small.

Similarly, for decomposition, we can write:

$$\begin{aligned} \mathbf{v} &= \mathbf{D}^{-1} \mathbf{b} \\ &= (\hat{\mathbf{g}}_P \quad \hat{\mathbf{g}}_{SH} \quad \hat{\mathbf{g}}_{SV})^T (\mathbf{b}_P + \mathbf{b}_{SH} + \mathbf{b}_{SV}) \end{aligned} \quad (\text{B3})$$

where, from equation (A2),  $\hat{\mathbf{g}}_M = \mathbf{J} \hat{\mathbf{b}}_M$ .

Equation (B3) can be evaluated directly, using appropriate reference velocities to compute  $\hat{\mathbf{g}}_P$  and  $\hat{\mathbf{g}}_{SV}$  - where again  $\hat{\mathbf{g}}_{SH}$  is parameter free and decouples. as for the composition equation,  $\hat{\mathbf{g}}_P$  is evaluated with the correct  $\alpha$ , but a possibly incorrect  $\beta$ , constrained by the average  $V_P / V_S$  ratio. In terms of reference vectors, they are written (c.f. equation B2)

$$\hat{\mathbf{g}}_P(x, z, \omega) = \lambda_P \hat{\mathbf{g}}_{P,J} + (1 - \lambda_P) \hat{\mathbf{g}}_{P,J+1}, \quad (\text{B4a})$$

and 
$$\hat{\mathbf{g}}_{SV}(x, z, \omega) = \lambda_S \hat{\mathbf{g}}_{SV,K} + (1 - \lambda_S) \hat{\mathbf{g}}_{SV,K+1}. \quad (\text{B4b})$$

The result, taking into account the decoupling of the SH mode, will be

$$\mathbf{v} = \begin{pmatrix} \hat{\mathbf{g}}_P^T \mathbf{b}_P \\ 0 \\ \hat{\mathbf{g}}_{SV}^T \mathbf{b}_P \end{pmatrix} + \begin{pmatrix} 0 \\ \hat{\mathbf{g}}_{SH}^T \mathbf{b}_{SH} \\ 0 \end{pmatrix} + \begin{pmatrix} \hat{\mathbf{g}}_P^T \mathbf{b}_{SV} \\ 0 \\ \hat{\mathbf{g}}_{SV}^T \mathbf{b}_{SV} \end{pmatrix}. \quad (\text{B5})$$

The cross-over terms  $\hat{\mathbf{g}}_P^T \mathbf{b}_{SV}$  and  $\hat{\mathbf{g}}_{SV}^T \mathbf{b}_P$  correspond to mode converted energy. Alternatively, the mode conversions can be neglected, to give

$$\mathbf{v}' = \begin{pmatrix} \hat{\mathbf{g}}_P^T \mathbf{b}_P \\ \hat{\mathbf{g}}_{SH}^T \mathbf{b}_{SH} \\ \hat{\mathbf{g}}_{SV}^T \mathbf{b}_{SV} \end{pmatrix}. \quad (\text{B6})$$

Use of equation (B6) rather than (B5) essentially converts the elastic migration to a set of scalar migrations which handle transmission effects.

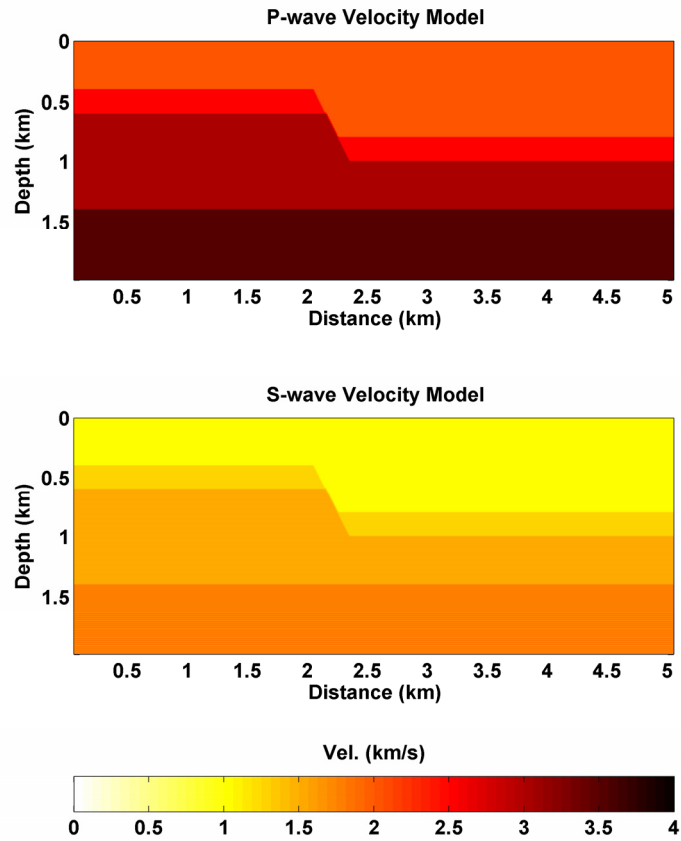


FIG. 2. Depth model used for migration example. Fault dips downwards at  $63.4^\circ$  angle. Isotropic VP and VS are shown here. For HTI example, second layer is replaced by HTI medium.

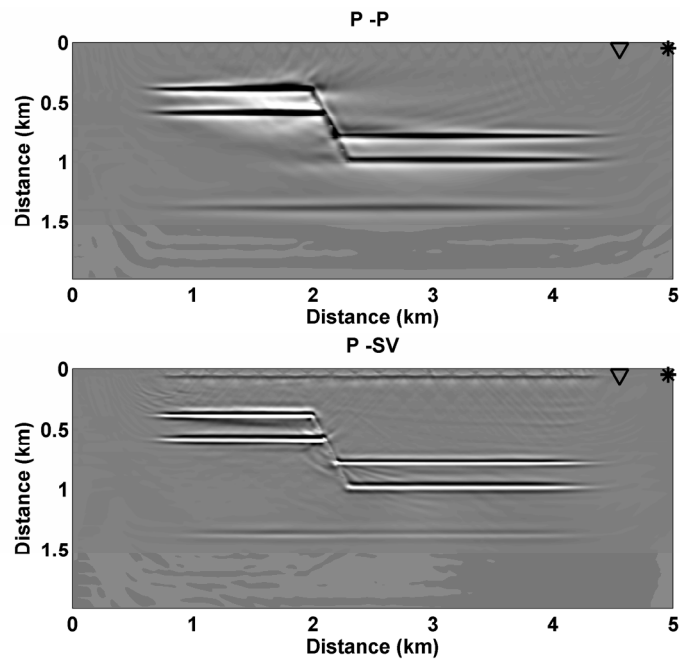


FIG. 3. PP and PS images from elastic wave-equation migration with of isotropic modeled data, from model shown in Figure 2.

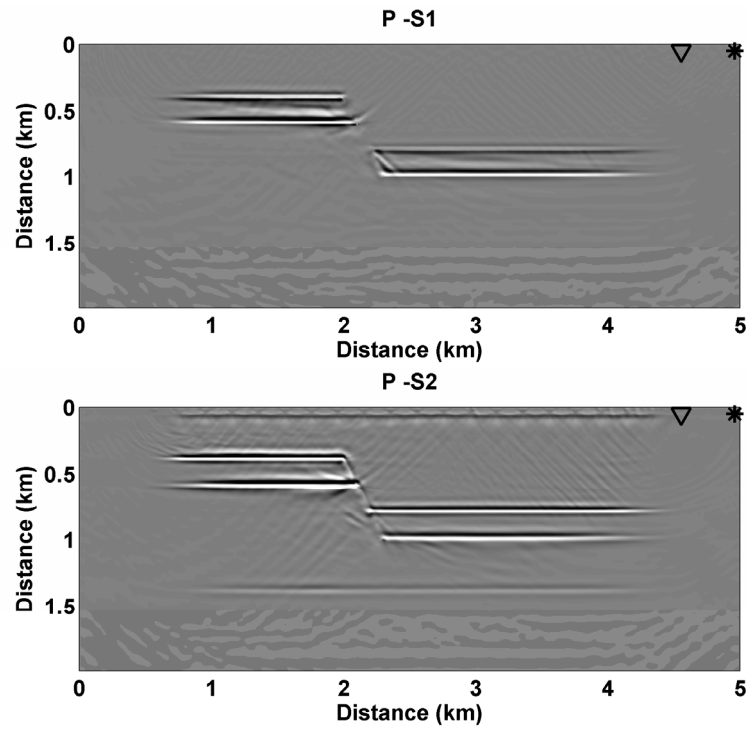


FIG. 4. PS1 and PS2 images from elastic wave-equation migration of HTI modelled data, with the model shown in Figure 2, but with an HTI second layer.

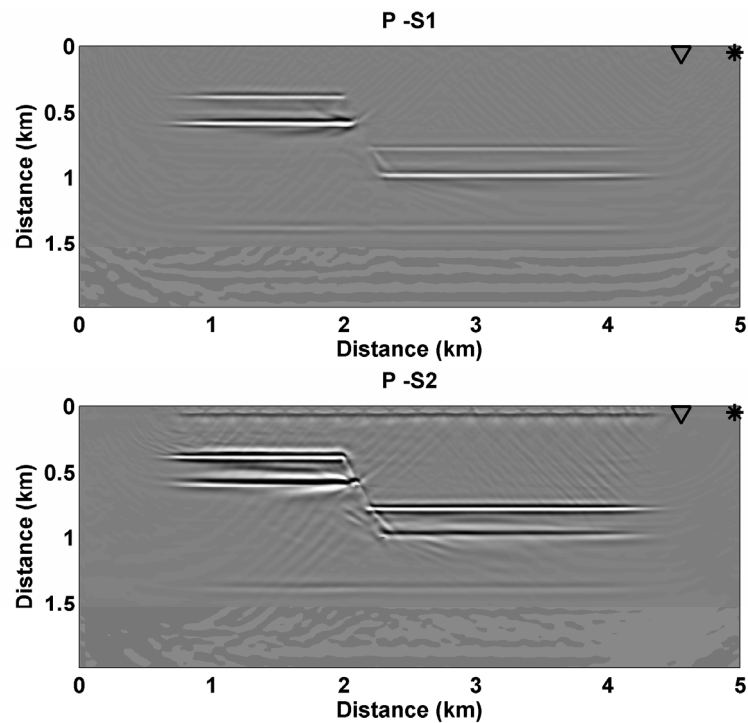


FIG. 5. PS1 and PS2 images from elastic wave-equation migration of HTI modeled data, using an isotropic model based upon the (vertical) P-wave and fast S-wave velocities. P-S1 corresponds to an S-wave polarized in the crossline direction, whereas P-S2 is polarized in the inline direction.

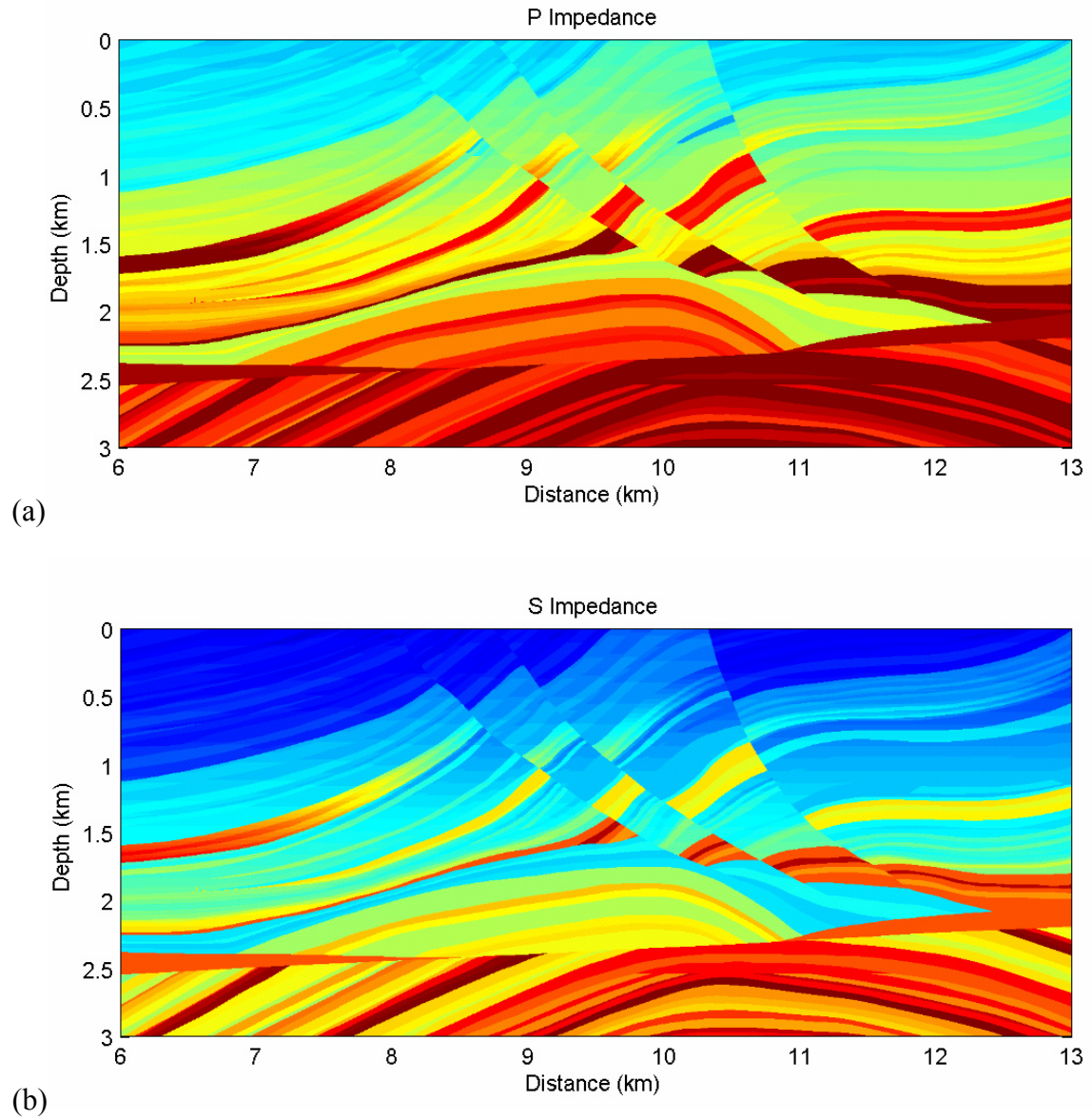


FIG. 6. Marmousi-2 elastic model, showing (a) acoustic (i.e. P-wave) impedance and (b) S-wave impedance. This area corresponds approximately to the original Marmousi acoustic model.

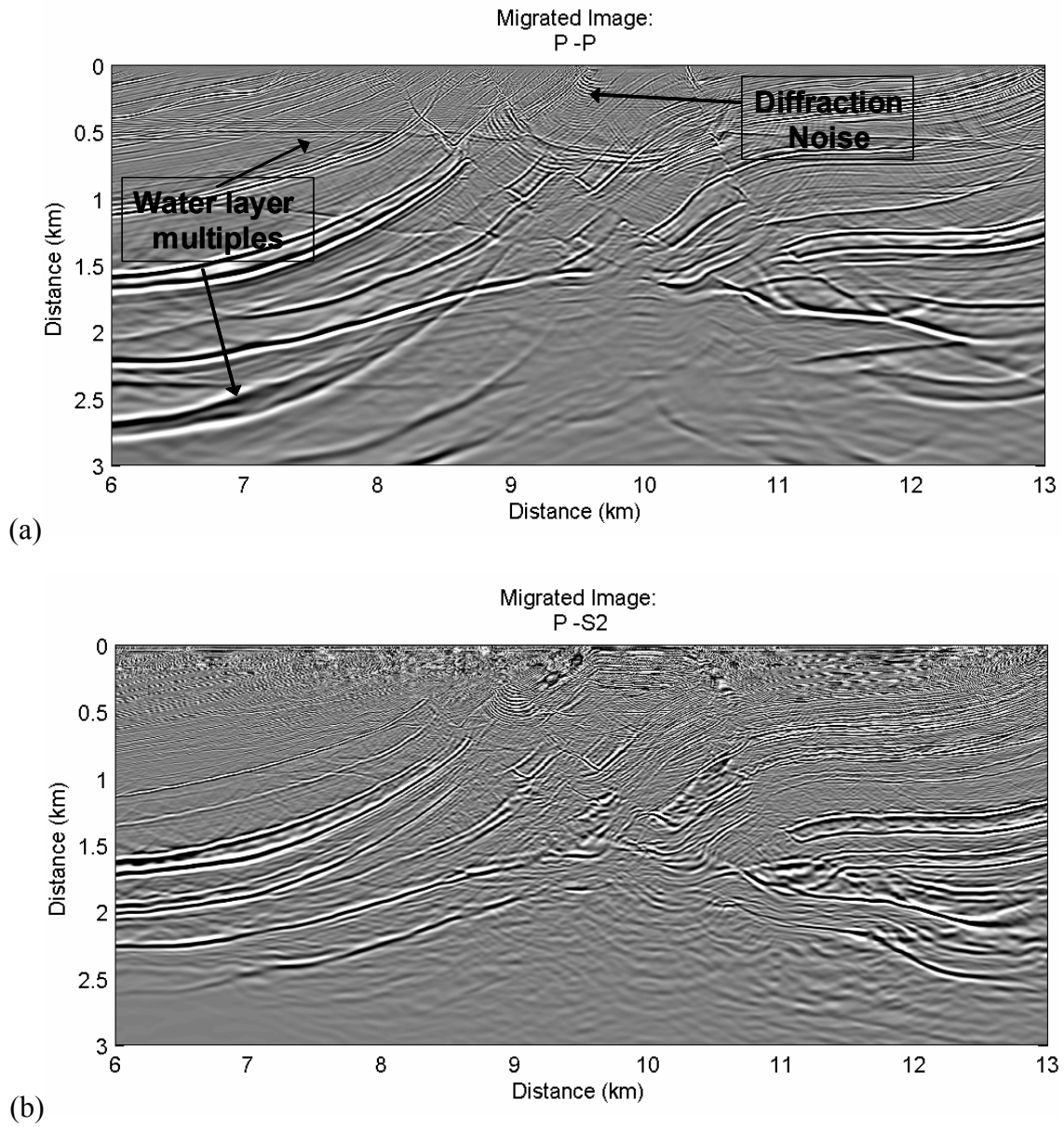


FIG. 7. Migrated images: (a) P-P and (b) P-S of X and Z component data from elastic modelling. Area shown is that of the model in figure 6.

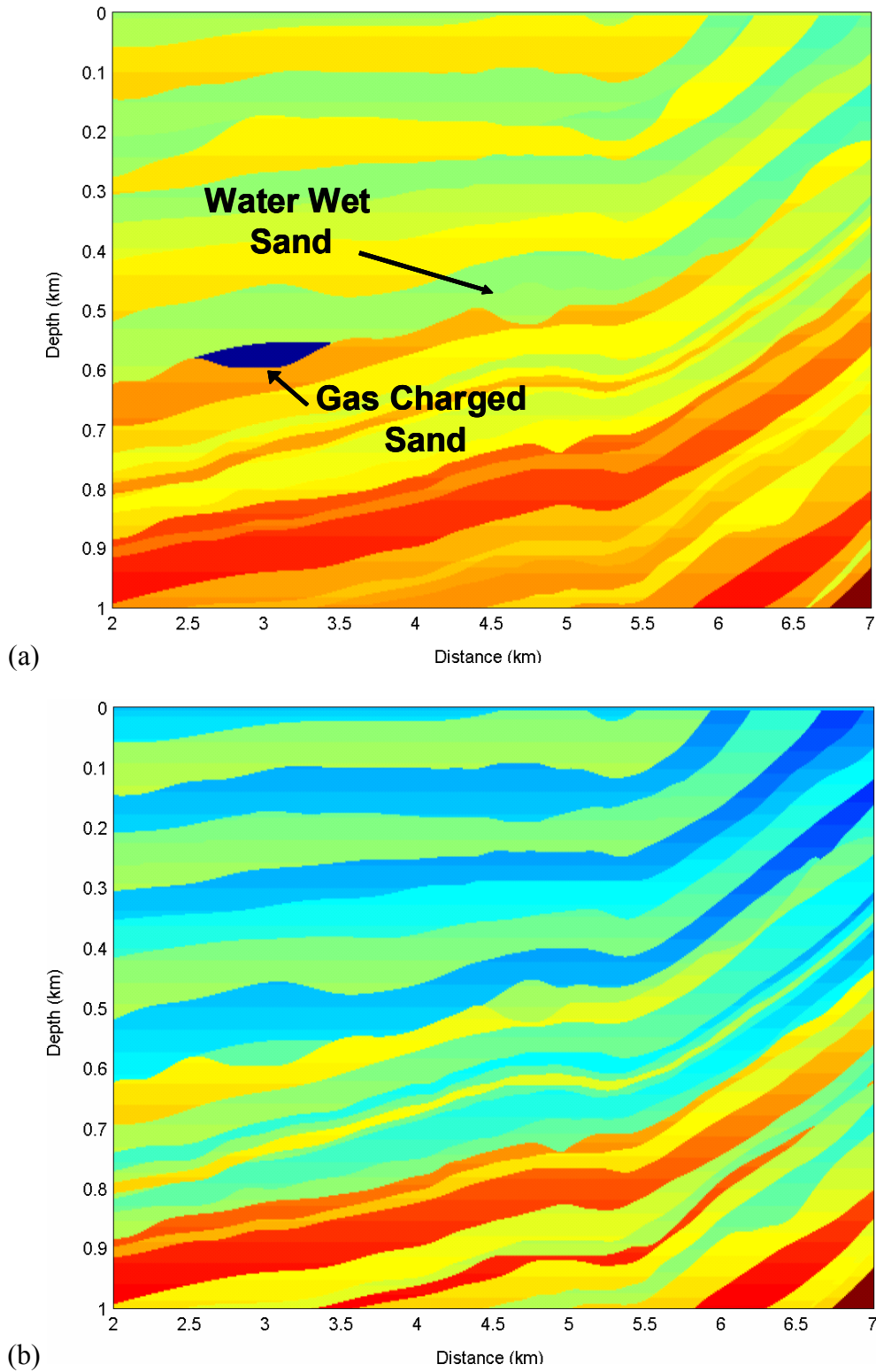


FIG. 8. Marmousi-2 elastic model, showing (a) acoustic (i.e. P-wave) impedance and (b) S-wave impedance. This area corresponds to a shallow section on the left of the main structural area. Note that the horizontal axis has been compressed relative to the vertical, for display purposes. The gas sand is clearly identified by its low P-wave impedance compared to local sediments.

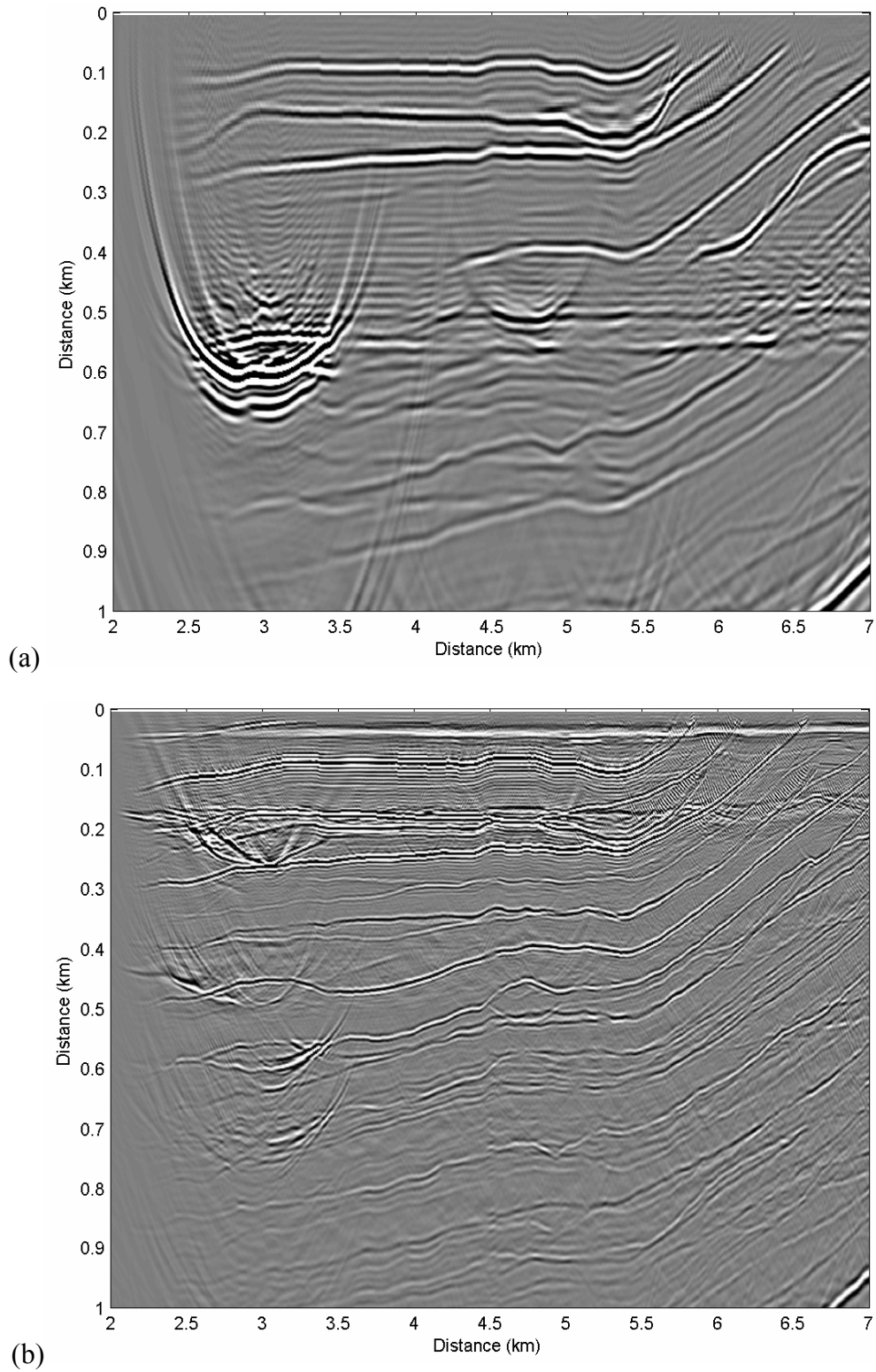


FIG. 9. Migrated images: (a) P-P and (b) P-S of X and Z component data from elastic modelling. Area shown is that of model in figure 8. Note the superior resolution of the P-S image, and the significantly weaker response to the gas sand. This is an example of fluid-lithology discrimination with elastic waves.